Mon. Not. R. Astron. Soc. **408,** 2008–2021 (2010) doi:10.1111/j.1365-2966.2010.17262.x

Ram pressure stripping in a galaxy formation model – I. A novel numerical approach

Tomás E. Tecce,[1,2★] Sofía A. Cora,[2,3] Patricia B. Tissera,[1,2] Mario G. Abadi[2,4] and Claudia del P. Lagos[5,6]

[1] *Instituto de Astronomía y Física del Espacio, C.C. 67 Suc. 28, C1428ZAA Ciudad de Buenos Aires, Argentina*
[2] *Consejo Nacional de Investigaciones Científicas y Técnicas, Rivadavia 1917, C1033AAJ Ciudad de Buenos Aires, Argentina*
[3] *Facultad de Ciencias Astronómicas y Geofísicas, Universidad Nacional de La Plata, and Instituto de Astrofísica de La Plata (CCT La Plata, CONICET, UNLP), Observatorio Astronómico, Paseo del Bosque S/N, B1900FWA La Plata, Argentina*
[4] *Instituto de Astronomía Teórica y Experimental and Observatorio Astronómico, Universidad Nacional de Córdoba, Laprida 854, X5000BGR Córdoba, Argentina*
[5] *Department of Physics, Institute for Computational Cosmology, University of Durham, South Road, Durham DH1 3LE*
[6] *Departamento de Astronomía y Astrofísica, Pontificia Universidad Católica de Chile, Av. Vicuña Mackenna 4860, Santiago, Chile*

Accepted 2010 June 28. Received 2010 May 28; in original form 2010 March 19

ABSTRACT

We develop a new numerical approach to describe the action of ram pressure stripping (RPS) within a semi-analytic model of galaxy formation and evolution which works in combination with non-radiative hydrodynamical simulations of galaxy clusters. The new feature in our method is the use of the gas particles to obtain the kinematical and thermodynamical properties of the intragroup and intracluster medium (ICM). This allows a self-consistent estimation of the RPS experienced by satellite galaxies. We find that the ram pressure in the central regions of clusters increases approximately one order of magnitude between $z = 1$ and 0, consistent with the increase in the density of the ICM. The mean ram pressure experienced by galaxies within the virial radius increases with decreasing redshift. In clusters with virial masses $M_{\rm vir} \simeq 10^{15}\,h^{-1}\,{\rm M}_{\odot}$, over 50 per cent of satellite galaxies have experienced ram pressures $\sim 10^{-11}\,h^{-2}\,{\rm dyn\,cm}^{-2}$ or higher for $z \lesssim 0.5$. In smaller clusters ($M_{\rm vir} \simeq 10^{14}\,h^{-1}\,{\rm M}_{\odot}$) the mean ram pressures are approximately one order of magnitude lower at all redshifts. RPS has a strong effect on the cold gas content of galaxies for all cluster masses. At $z = 0$, over 70 per cent of satellite galaxies within the virial radius are completely depleted of cold gas. For the more massive clusters the fraction of depleted galaxies is already established at $z \simeq 1$, whereas for the smaller clusters this fraction increases appreciably between $z = 1$ and 0. This indicates that the rate at which the cold gas is stripped depends on the virial mass of the host cluster. Compared to our new approach, the use of an analytic profile to describe the ICM results in an overestimation of the ram pressure larger than 50 per cent for $z > 0.5$.

Key words: galaxies: clusters: general – galaxies: clusters: intracluster medium – galaxies: evolution – galaxies: formation – intergalactic medium.

1 INTRODUCTION

Comparison between galaxies in clusters and in the field reveals remarkable differences in their physical properties, which suggest the important influence of environment on galaxy formation and evolution. Large galaxy surveys have shown that the colour distribution of the galaxy population is clearly bimodal (Strateva et al. 2001; Baldry et al. 2004). One peak is formed by red, non-star-forming galaxies, while the other is populated by blue galaxies with active star formation. In the local Universe, the fraction of red sequence galaxies at a given stellar mass depends on environment (Balogh et al. 2004; Baldry et al. 2006), with galaxy clusters having larger fractions of red, early-type galaxies than the field. Environment also influences the star formation rates (SFRs) of galaxies, as these are strongly suppressed in dense environments for galaxies over a large range of stellar masses (e.g. Kauffmann et al. 2004).

Another quantity that shows dependence on environment is galaxy morphology. Spiral galaxies tend to be rarer in the central regions of clusters than early-type galaxies (Dressler 1980;

★E-mail: tomas@iafe.uba.ar

Whitmore, Gilmore & Jones 1993), and cluster spiral galaxies differ from those in the field in several characteristics that can be correlated with environment (for an extensive review see Boselli & Gavazzi 2006). In clusters, spiral galaxies are not only redder but also more H I deficient than similar galaxies in the field, with this deficiency increasing for galaxies closer to the cluster centre (Haynes, Giovanelli & Chincarini 1984; Solanes et al. 2001; Hughes & Cortese 2009). In field spirals the gaseous discs typically extend beyond the optical radius, but the opposite trend is seen in clusters, where a significant fraction of spirals have truncated gaseous discs (e.g. Koopmann & Kenney 2004, 2006; Koopmann, Haynes & Catinella 2006).

A likely scenario is that galaxies are transformed from blue star-forming systems into the red and passive population, but it is still unclear which physical processes are the key ones responsible for this transformation, and what their relative importance may be. The observed differences between cluster and field galaxies outlined above suggest that the transformation could be the result of processes that remove gas from galaxies, suppressing their star formation, and/or alter the galaxy morphology, both effects happening preferentially in high-density environments. Galaxy–galaxy interactions and mergers are among these possible mechanisms as suggested by some theoretical (Moore et al. 1996; Perez et al. 2006a,b) and observational (e.g. Ellison et al. 2008, 2010; Perez et al. 2009) results. Moore et al. (1996, 1999) proposed that the evolution of galaxies in groups and clusters is governed by the combined action of multiple close encounters between galaxies and the tidal interaction with the group potential, a process that they call 'galaxy harassment'. In clusters, however, the relative velocities of galaxies are higher than in galaxy groups and, consequently, the interaction times are shorter (Mihos 2004), so this process is expected to be more significant in less dense environments.

Another process that might be relevant is the removal of the hot diffuse gas halo of a galaxy after its infall into a group or cluster. This has been called 'strangulation' or 'starvation' (Larson, Tinsley & Caldwell 1980; Balogh, Navarro & Morris 2000; Kawata & Mulchaey 2008). The removed gas becomes part of the overall intragroup or intracluster medium (ICM), the affected galaxy cannot accrete any more gas via cooling flows, and with a moderate SFR it will consume all of its cold gas within a few Gyr, ending its star formation and becoming gradually redder as its stellar population ages. Strangulation is a standard ingredient in most semi-analytic models of galaxy formation, which successfully reproduce observed global properties of galaxies such as luminosity functions, colour distributions and mass–metallicity relations (e.g. Baugh, Cole & Frenk 1996; Springel et al. 2001; Bower et al. 2006; Croton et al. 2006; Lagos, Cora & Padilla 2008, hereafter LCP08). As commonly implemented, as soon as a galaxy becomes a satellite, its hot gas halo is assumed to be shock heated to the virial temperature of the group and immediately removed from the galaxy. This effect proceeds in the same fashion in groups of all masses.

Ram pressure stripping (RPS) of the cold gas in galactic discs could also play an important role. Galaxies in clusters move through the hot diffuse ICM gas at velocities that could be close to supersonic (Faltenbacher & Diemand 2006), and so will experience considerable ram pressure (RP). Gunn & Gott (1972, hereafter GG72) proposed that when the RP exceeds the gravitational restoring force of the galaxy, its cold gas will be pushed out. In recent years, RPS has been extensively studied using hydrodynamical simulations of individual galaxies (e.g. Abadi, Moore & Bower 1999; Quilis, Moore & Bower 2000; Marcolini, Brighenti & D'Ercole 2003; Roediger & Brüggen 2006, 2007; Kronberger et al. 2008) which suggest that the GG72 estimate is a fairly good approximation in most situations, and that the time-scale for gas removal is ∼10–100 Myr. RPS acts only on the gaseous components of the galaxy, so its characteristic signature is the presence of truncated gas discs while the stellar discs remain unaltered. Indeed, there are several observational candidates for RPS (e.g. Crowl et al. 2005; Boselli et al. 2006; Cortese et al. 2007; Sun, Donahue & Voit 2007; Vollmer 2009). RPS also seems to be relevant for dwarf galaxies in less dense environments, such as galaxy groups (McConnachie et al. 2007; Mastropietro, Burkert & Moore 2008). A recent review of both simulations and observations of RPS can be found in Roediger (2009).

All the physical processes described above are not mutually exclusive. In a hierarchical universe, many galaxies in clusters were previously members of smaller systems where a combination of strangulation, harassment and/or RPS could start to suppress star formation (this has been called 'galaxy pre-processing'; see e.g. Fujita 2004; Mihos 2004; Cortese et al. 2006; Perez et al. 2009).

Semi-analytic models of galaxy formation include galaxy mergers and strangulation as standard elements, but the effect of RPS has been included in such models only in few cases (Okamoto & Nagashima 2003; Lanzoni et al. 2005) where no significant influence of RPS was found on the analysed galaxy properties. These previous works use dark matter (DM)-only simulations to generate the merging history trees of DM haloes, which are then used by the semi-analytic model to generate the galaxy population, and the properties of the ICM and velocity distributions of galaxies are modelled using analytical approximations.

A more recent work by Brüggen & De Lucia (2008, hereafter BDL08) studies the distribution and history of the RP experienced by galaxies in clusters, combining a semi-analytic model with the Millennium Simulation (Springel et al. 2005); they use the properties of the DM particles to track the positions and velocities of simulated galaxies. Again, since the Millennium is a DM-only simulation, BDL08 have to resort to analytic models for the ICM properties, assuming the hypothesis of hydrostatic equilibrium for the gas within a DM halo described by the Navarro, Frenk & White (1997, hereafter NFW) profile. The latter is a good approximation to the DM profiles if the haloes are in dynamical equilibrium; this is likely not the case for high-redshift haloes, where the bulk of the star formation activity takes place (e.g. Madau et al. 1996; Ciardi, Stoehr & White 2003; Hopkins 2007). Since the dynamics of the ICM may play an important role (Sunyaev, Norman & Bryan 2003) and certainly the hypothesis of hydrostatic equilibrium may not hold for all haloes, our aim is to develop an improved model for RPS which takes into account the ICM dynamics through simulations that include gas physics.

We model RPS by adopting the criterion proposed by GG72 and by implementing this process in the semi-analytic model of galaxy formation and evolution, Semi-Analytic Galaxies (SAG; LCP08), which is combined with hydrodynamical cosmological simulations of galaxy clusters (Dolag et al. 2005). The novel feature of our implementation is the fact that the thermodynamical and kinematical properties of the ICM, which are involved in the estimations of the RP experienced by each galaxy, are provided by the underlying simulations. In this paper, the first of a series, we focus on the study of the distributions of RP experienced by satellite galaxies in clusters of different masses, the dependence of RP with clustercentric distance and how these quantities evolve with redshift. We compare our results with those obtained by assuming NFW profiles for the density distribution of the ICM. A forthcoming paper will deal with the influence of RPS on galaxy properties such as luminosities, colours and star formation histories.

This paper is organized as follows. In Section 2, we briefly describe the semi-analytic model SAG used in this work and give details of the simulations used. Section 3 contains a detailed description of the way in which RP is estimated from the hydrodynamical simulations, and the implementation of the RPS process in the semi-analytic model. Section 4 presents the distributions of RP that we obtain from our cluster simulations and compare them to the results obtained by adopting a NFW profile for the ICM under the hypothesis of hydrostatic equilibrium. We then analyse the effects of RPS on the gas content of galaxies. Finally, in Section 5 we summarize our main findings.

2 NUMERICAL SIMULATIONS AND THE SEMI-ANALYTIC MODEL

To develop our RPS model we use a hybrid numerical approach which combines cosmological non-radiative N-body/smoothed particle hydrodynamics (SPH) simulations of galaxy clusters with a semi-analytic model of galaxy formation and evolution. In the cosmological simulation, the DM haloes and their substructures are identified and followed in time, building up detailed merger trees which are used by the semi-analytic code to generate the galaxy population. The main advantage of this hybrid procedure is that the use of semi-analytic codes allows the exploration of a larger dynamical range than fully self-consistent simulations, at a fraction of the computational cost.

In the present work we implement the RPS process in the semi-analytic code developed by LCP08. We take the kinematical and thermodynamical properties of the hot diffuse gas which permeates DM haloes directly from the underlying SPH simulation, thus avoiding the use of analytical approximations. In this section, we briefly describe the simulations and the semi-analytic model on to which we graft our RPS scheme described in detail in Section 3.

2.1 Non-radiative N-body/SPH simulations of galaxy clusters

In this study, we use the high-resolution hydrodynamic non-radiative simulations of galaxy clusters by Dolag et al. (2005). The simulated clusters were originally extracted from a DM-only simulation with a box size of $479\,h^{-1}$ Mpc of a flat Λ cold dark matter (ΛCDM) model with $\Omega_{\rm m} = 0.3$, $\Omega_\Lambda = 0.7$, $H_0 = 100\,h^{-1}\,{\rm km\,s^{-1}\,Mpc^{-1}}$, where $h = 0.7$, a baryon density $\Omega_{\rm b} = 0.039$ and a normalization of the power spectrum $\sigma_8 = 0.9$ (Yoshida, Sheth & Diaferio 2001). The Lagrangian regions surrounding the selected clusters have been resimulated at higher mass and force resolution using the 'zoomed initial conditions' technique (Tormen, Bouchet & White 1997). Gas was introduced in the high-resolution region by splitting each parent particle into a gas and a DM particle. The mass resolution is the same for all simulations, being $m_{\rm DM} = 1.13 \times 10^9\,h^{-1}\,{\rm M}_\odot$ for DM particles and $m_{\rm gas} = 1.69 \times 10^8\,h^{-1}\,{\rm M}_\odot$ for gas particles. However, the identification of DM haloes was based only on the DM particles, with their mass increased to its original value.

The simulations have been carried out using GADGET-2, a parallel Tree-SPH code with fully adaptive time-stepping and explicit conservation of energy and entropy (Springel 2005). For the force resolution, the gravitational softening is fixed at $\epsilon = 5\,h^{-1}$ kpc in physical units at $z \leq 5$, and for higher redshifts it shifts to $\epsilon = 30\,h^{-1}$ kpc in comoving units. For each simulation, 92 snapshots were stored between redshifts $z = 60$ and 0. The simulations considered here include only non-radiative physics and the original formulation of artificial viscosity within SPH; this is a reasonable approximation for simulations of clusters, since the bulk of the halo gas has very long cooling times.

From these simulations, we have selected eight cluster-sized haloes divided in two sets: five clusters with $M_{\rm vir} \simeq 10^{14}\,h^{-1}\,{\rm M}_\odot$ (hereafter G14 clusters) and three clusters with $M_{\rm vir} \simeq 10^{15}\,h^{-1}\,{\rm M}_\odot$ (hereafter G15 clusters). These DM haloes are first identified in the simulation outputs by means of a friends-of-friends (FOF) algorithm (Davis et al. 1985). Subsequently, the SUBFIND algorithm (Springel et al. 2001) is applied to the haloes detected by FOF in order to find self-bound DM substructures which we call *subhaloes*. To build the trees, we extract from the simulations all subhaloes consisting of 10 or more DM particles, since smaller ones are usually dynamically unstable (Kauffmann et al. 1999). Additionally, SPH particles in the simulations provide the density, spatial and velocity distributions of the intergalactic and intracluster media.

2.2 Semi-analytic model of galaxy formation

The DM halo merger trees and the information from the SPH particles are then used as input for the semi-analytic model of galaxy formation SAG (LCP08), based on the one described by Cora (2006), which includes the effects of radiative cooling of hot gas, star formation, feedback from supernovae explosions, chemical enrichment and galaxy mergers. SAG includes the effect of strangulation as described in the Introduction. LCP08 updated it to include black hole (BH) growth and feedback from active galactic nuclei (AGN). In addition to this major improvement, SAG allows starbursts in three different ways: both in major and minor mergers, and when disc instabilities occur. The reader is referred to Cora (2006) and LCP08 for the full details of these implementations. In the present work, this model is further modified to include the effect of RPS on galaxies due to the hot intergalactic gas as described in the next section.

The galaxy catalogue is built up by applying the semi-analytic model to the detailed DM subhalo merger trees extracted from the hydrodynamical simulations. Similarly to other semi-analytic models, in this 'subhalo scheme' arising from the identification of DM substructures within FOF groups, the largest subhalo in a FOF group is assumed to host the central galaxy of the group, located at the position of the most bound particle of the subhalo. These galaxies are designated as *central* or *type 0* galaxies, and each FOF halo has only one. Central galaxies of smaller subhaloes contained within the same FOF group are referred to as *halo* or *type 1* galaxies. The subhaloes of these galaxies are still intact after falling into larger structures. There is a third group of galaxies generated when two subhaloes merge and the galaxy of the smaller one becomes a satellite of the remnant subhalo: these galaxies are called *type 2* galaxies. A type 0 galaxy can have satellites of types 1 and 2 and, furthermore, a type 1 galaxy may itself have type 2 satellites. In the following, whenever we use the term 'satellite galaxies' we will be referring to both type 1 and type 2 galaxies. We assume that type 2 galaxies merge with their corresponding subhalo central galaxy on a dynamical friction time-scale.

For each of these galaxies, SAG provides information on the stellar mass, cold disc gas, hot gas within DM haloes, BH mass, AGN activity, star formation histories, magnitudes in several bands according to the stellar population models by Bruzual & Charlot (2003) and chemical abundances of the different baryonic components. Galaxy positions and velocities are traced by tracking the position and velocity of the most bound particle of their host DM subhalo; for type 2 galaxies, we use the most bound particle identified at the last time there was a substructure (as in BDL08). In a forthcoming paper we will test how the effect of RPS depends on the choice of alternative recipes for the different physical processes such as the star formation scheme and the galaxy orbits.

3 RAM PRESSURE STRIPPING OF COLD DISC GAS

In this section we describe our self-consistent implementation of RPS in the semi-analytic code. Our RPS model is based on the simple criterion proposed by GG72: the cold gas of the galactic disc located beyond galactocentric radius R will be stripped away if the RP exerted by the ambient medium on the galaxy exceeds the restoring force per unit area due to the gravity of the disc:

$$\rho_{\rm ICM} v^2 \geq 2\pi G \Sigma_{\rm disc}(R)\Sigma_{\rm cold}(R). \qquad (1)$$

Here $\rho_{\rm ICM}$ is the ambient density of the ICM at the current position of the galaxy, v the velocity of the galaxy relative to the ICM and $\Sigma_{\rm disc}$, $\Sigma_{\rm cold}$ are the surface densities of the galactic disc (stars plus cold gas) and of the cold gas disc, respectively. Although the description of RP phenomena is usually quoted in the context of galaxy clusters, it is valid in general, and we apply this criterion to the hot gas contained within all DM haloes at all redshifts.

In order to determine the RPS, we need an estimation of each of the parameters involved in condition (1), namely the properties of the ICM on the left-hand side and the scalelength of the galactic discs necessary to evaluate the right-hand side. Below, we explain the strategies used to estimate these quantities within our hybrid model.

3.1 Determination of the ICM properties

As already mentioned in the Introduction, the main difference between our RPS implementation in a semi-analytic model and previous ones (Okamoto & Nagashima 2003; Lanzoni et al. 2005) is that we use the thermodynamical properties of the ICM derived from the underlying hydrodynamical simulation. For all satellite galaxies in the simulations, we determine the local ICM density $\rho_{\rm ICM}$ and velocity v relative to the ICM by searching for all gas particles in a sphere of radius $r_{\rm ngb} \propto r_{\rm vir}$ centred on each galaxy, where $r_{\rm vir}$ is the virial radius of the host DM subhalo of the satellite. For type 2 galaxies, the value of $r_{\rm vir}$ corresponds to the last time the galaxy was identified as either type 0 or type 1. If less than 32 particles are found, we take the closest 32 neighbours instead.

Some of the particles selected by this procedure might be gravitationally bound to the DM subhalo. In such a case, ICM densities would be overestimated, and the velocity of the galaxy relative to the mean ICM would artificially be $v \sim 0$. Thus, these particles need to be discarded since we are interested in estimating the properties of the ambient medium which is responsible for the RPS. To do this, once all gas neighbour particles have been found, the higher density ones are filtered out by using an iterative procedure: we determine the median gas density $\rho_{\rm m}$ of the selected particles, discard all particles with $\rho > f_{\rm rm}\rho_{\rm m}$ and repeat this procedure until the median density converges. We find that choosing $r_{\rm ngb} = 2.5\ r_{\rm vir}$ and $f_{\rm rm} = 2$, a smooth ICM density distribution can be recovered, removing substructure in the gas without significantly affecting the median density profile. The final step is then to determine the velocity v of the galaxy relative to the mean motion of the gas particles that remain after filtering.

By calculating the ICM properties in this fashion, we obtain a self-consistent method which does not introduce any additional free parameter into the model and does not need to assume that the ICM gas is in hydrostatic equilibrium. In fact, it automatically takes into account any local variation of the density and/or the velocity field due to the dynamics of the gas. The method is not overly sensitive to the values of $f_{\rm rm}$ and $r_{\rm ngb}$ chosen; $r_{\rm ngb}$ is a compromise between the need to consider a radius large enough to obtain a fair sample of the local environment, but not so large that the search spans a large portion of the cluster volume. With $f_{\rm rm} > 3$ the method becomes ineffective at removing substructure, and choosing $f_{\rm rm} \leq 1$ the method underestimates the median ICM density when compared to observations.

The density profiles we obtain from this procedure, for the case of the cluster-sized haloes, are in excellent agreement with those determined from X-ray observations of galaxy clusters at $z \simeq 0$ (e.g. Schindler, Binggeli & Böhringer 1999; Vikhlinin et al. 2006). This can be seen in the top panel of Fig. 1, where we compare the mean ICM density profiles obtained for the simulated clusters with the profiles obtained by Vikhlinin et al. (2006) for a sample of nearby relaxed clusters, which span a temperature range 0.7–9 keV that comprises the mass-weighted temperatures of the simulated clusters (see Dolag et al. 2005).

3.2 Sizes of galactic discs

In the semi-analytic code SAG, the gas acquired by a galaxy via cooling flows is assumed to settle on to a thin exponential disc with surface density $\Sigma(R) = \Sigma_0 \exp(-R/R_{\rm d})$, where Σ_0 is the central surface density and $R_{\rm d}$ the disc scalelength. If the outer disc radius $R_{\rm disc} \gg R_{\rm d}$, then these quantities are related to the total disc mass $M_{\rm d}$ through

$$\Sigma_0 = \frac{M_{\rm d}}{2\pi R_{\rm d}^2}. \qquad (2)$$

To determine the disc scalelength we follow the model developed by Mo, Mao & White (1998, hereafter MMW). Assuming a NFW profile to represent the DM distribution, the MMW model allows the calculation of $R_{\rm d}$ given the halo virial mass $M_{\rm vir}$, the mass fraction of baryons that settle on to the disc $m_{\rm d} = M_{\rm d}/M_{\rm vir}$, the halo concentration c and the dimensionless halo spin parameter $\lambda = J|E|^{1/2}G^{-1}M_{\rm vir}^{-5/2}$, where J and E are the angular momentum and energy of the halo, respectively.

The MMW model assumes that the DM halo responds adiabatically to the slow assembly of the disc, following the standard scheme of Blumenthal et al. (1986). The initial NFW mass profile $M(r_{\rm i})$ and the profile after contraction $M_f(r)$ are then related by

$$M_f(r) = M_{\rm d}(r) + M_{\rm b} + M(r_{\rm i})(1 - m_{\rm d} - m_{\rm b}), \qquad (3)$$

where $M_{\rm b}$ is the total bulge mass (considering bulges as point masses, for simplicity), $m_{\rm b} = M_{\rm b}/M_{\rm vir}$, and $M_{\rm d}(r)$ is the disc mass within r given by

$$M_{\rm d}(r) = 2\pi\Sigma_0 R_{\rm d}^2 \left[1 - \left(1 + \frac{r}{R_{\rm d}}\right)\exp(-r/R_{\rm d})\right]. \qquad (4)$$

The implicit assumption is that the initial distribution of baryons parallels that of the DM, and those that do not end up in the disc or in the bulge remain distributed in the same way as the DM. These considerations allow MMW to express the disc scalelength as

$$R_{\rm d} = \frac{1}{\sqrt{2}}\left(\frac{j_{\rm d}}{m_{\rm d}}\right)\lambda\, r_{\rm vir} f_c^{-1/2} f_R(\lambda, c, m_{\rm d}, j_{\rm d}), \qquad (5)$$

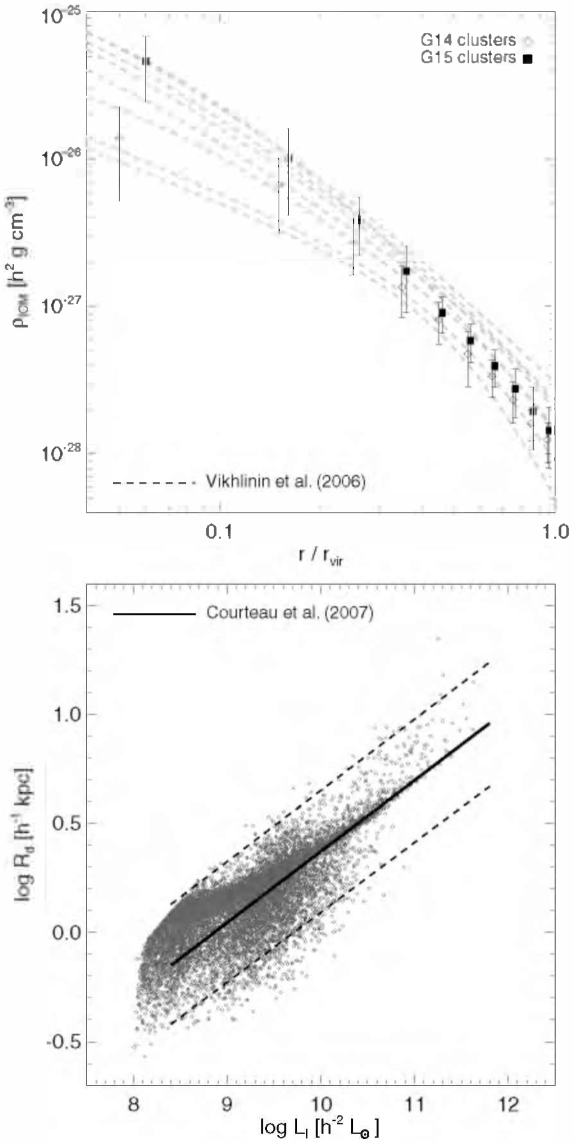

Figure 1. Top: mean ICM density profiles of the simulated clusters at $z = 0$. Open diamonds and filled squares show values for the G14 and G15 clusters, respectively. Data points for the G15 clusters are shifted to the right for clarity. Dashed lines show the average density profiles determined by Vikhlinin et al. (2006) for a sample of nearby relaxed clusters. Bottom: relation between disc scalelength $R_{\rm d}$ and I-band luminosity for disc galaxies, for a run of the SAG model that includes the RPS effect. We selected galaxies with $M_{\rm baryon} \geq 10^8\, h^{-1}\, {\rm M}_{\odot}$, $M_{\rm bulge}/M_{\rm stellar} \leq 0.95$ and with central surface brightness $\mu_0(B) < 22\,{\rm mag\,arcsec}^{-2}$. For this plot we take all the galaxies in one of the largest simulation boxes, including both cluster-sized haloes and smaller systems. Solid and dashed lines show the mean observed relation and 2σ scatter from Courteau et al. (2007).

where $j_{\rm d} = J_{\rm d}/J$, with $J_{\rm d}$ the total disc angular momentum, and f_c, f_R are factors given by

$$f_c \simeq \frac{2}{3} + \left(\frac{c}{21.5}\right)^{0.7}, \tag{6}$$

$$f_R(\lambda, c, m_{\rm d}, j_{\rm d}) = 2\left[\int_0^{\infty} {\rm e}^{-u} u^2 \frac{V_{\rm c}(R_{\rm d}u)}{V_{\rm vir}}\, {\rm d}u\right]^{-1} \tag{7}$$

(see MMW for the full details). If the specific angular momentum of the disc material is the same as that of the parent halo, then the ratio $j_{\rm d}/m_{\rm d}$ should be close to unity (Fall & Efstathiou 1980). Thus, we set $j_{\rm d} = m_{\rm d}$ and assume the angular momentum of the bulge to be negligible.

For a given set of values of $V_{\rm vir}, c, \lambda, m_{\rm d}$ and $j_{\rm d}$, equations (3)–(7) must be solved by iteration to yield $R_{\rm d}$. However, including this iterative method in the semi-analytic model is extremely time consuming. Most semi-analytic models use a fitting formula for $R_{\rm d}$ determined by MMW (their equation 32), but this is valid only for the case of pure disc galaxies and with an accuracy of 15 per cent quoted only for values of $m_{\rm d}$ in the range $0.02 < m_{\rm d} < 0.2$. We find that galaxies in our simulations cover a much broader range in $m_{\rm d}$; besides, we also want to take into account the presence of bulges and their gravitational effect on the size of the final disc. Hence, we use the iterative procedure to generate a set of look-up tables for each snapshot of the underlying simulation and for a grid of values of $m_{\rm d}, m_{\rm b}, c$ and λ. These tables are then used by the semi-analytic model to find $R_{\rm d}$ by interpolation.

We assume that the process of disc formation takes place only for central galaxies. When a galaxy becomes a satellite, the accretion of cold gas is halted due to strangulation, so its disc cannot grow any further. We then take $R_{\rm d}$ to be frozen at the value it had at the last time the galaxy was identified as a central. Additionally, if a galaxy suffers a major merger or if the galactic disc becomes unstable, the remnant is a spheroid and so $R_{\rm d}$ is set equal to zero after such an event.

The values of $m_{\rm d}$ and $m_{\rm b}$ are calculated for each central galaxy from the properties given by the semi-analytic code. The concentration of their host DM haloes are determined as a function of $M_{\rm vir}$ and redshift by following the model by Bullock et al. (2001), with the parameters quoted by Wechsler et al. (2006). The spin parameter λ is determined for each halo by computing its total energy and angular momentum. Studies based in N-body simulations have found that the distribution of λ for DM haloes can be well described by a lognormal function with mean $0.03 \lesssim \lambda_0 \lesssim 0.05$ and dispersion $\sigma \simeq 0.5$ (e.g. Warren et al. 1992; Bett et al. 2007; Macciò et al. 2007). For the simulations used here $\lambda_0 = 0.042$, but the distribution deviates from the lognormal for high values of λ. This happens because the mass resolution in N-body simulations affects the determination of angular momenta, independently of the method used to find DM structure, generating an artificial high-λ tail in the distribution (Bett et al. 2007). The value of the spin parameter correlates with the degree of equilibrium of the DM halo, with haloes which are far from being virialized having large values of λ. As a consequence, we use the simple criterion proposed by Bett et al. (2007) to filter out these anomalous values. For each halo, we calculate an 'instantaneous virial ratio'

$$Q \equiv |2T/U + 1| \tag{8}$$

and consider that haloes with values $Q < 1$ are in a quasi-equilibrium state. This allows us to correct the distribution of λ for mass resolution effects. For central galaxies of anomalous haloes ($Q \geq 1$), we set $R_{\rm d} = \lambda_0 r_{\rm vir}/\sqrt{2}$ (MMW, their equation 12).

This procedure generates a distribution of sizes of galactic discs which is in good agreement with observations. The bottom panel of Fig. 1 shows the relation between disc scalelength and I-band luminosity, compared to the observed relation from Courteau et al. (2007). The data were extracted from a run of the SAG model which includes the RPS effect as described in Sections 3.1 and 3.3 (see also Section 4.2). The plot includes all galaxies with $M_{\rm baryon} \geq 10^8\, h^{-1}\, {\rm M}_{\odot}$ within one of the largest simulation boxes, comprising not only cluster-sized haloes but also smaller systems. We select as spirals those galaxies with central surface brightness

$\mu_0(B) < 22\,\mathrm{mag\,arcsec^{-2}}$ to exclude low surface brightness (LSB) systems (Impey, Burkholder & Sprayberry 2001), and with $r_{\rm thresh} \equiv M_{\rm bulge}/M_{\rm stellar} \leq 0.95$ (following LCP08). Varying $r_{\rm thresh}$ between 0.5 and 0.95 does not result in any significant change in the distribution of morphological types with galaxy stellar mass.

The agreement between the model and observations is very good both in terms of the slope and the scatter of the relation. For a given luminosity, galaxies with higher values of λ (i.e. with higher angular momentum) have larger discs. Once the artificially large values of λ have been corrected, very few galaxies (<5 per cent) fall in the region above the upper dashed line in Fig. 1, and those are mostly LSB galaxies. Disc galaxies are not found in the region below the lower dashed line (and below the mean for $L_I > 10^{11}\,h^{-2}\,\mathrm{L_\odot}$) because such discs become unstable.

3.3 Modelling ram pressure stripping

With the relevant properties of the ICM estimated as previously described we can now construct our RPS model. The mass loss due to RPS is calculated analytically as follows. For exponential discs of stars and gas, it can be shown from condition (1) that RPS will remove from a galaxy all the gas beyond a stripping radius $R_{\rm str}$ given by

$$R_{\rm str} = -0.5 R_{\rm d} \ln\left[\frac{\rho_{\rm ICM} v^2}{2\pi G \Sigma_{0,\rm disc}\Sigma_{0,\rm cold}}\right]. \tag{9}$$

Here $\Sigma_{0,\rm cold}$ and $\Sigma_{0,\rm disc}$ are the central surface densities of the cold gas disc and of the galactic disc. We assume, for simplicity, that both disc components (stars and cold gas) have the same scalelength. To avoid extremely large values of $R_{\rm str}$, which may lead to divergences in the calculations, we ignore the effect of RPS if $R_{\rm str}/R_{\rm d} \geq 20$; in such cases the fraction of gas removed is negligible.

Our calculation of mass loss follows that of Lanzoni et al. (2005). The previous study by Okamoto & Nagashima (2003) used a much rougher estimation of RPS: for each galaxy they calculated a mean gravitational restoring force, and if the RP exceeded its value, all the cold gas was removed; if the RP was smaller, no gas was lost. This is a crude assumption, and we consider the Lanzoni et al. (2005) approach a better representation of the continuous gas removal caused by RPS. A difference between our work and Lanzoni et al. (2005) is that they include a factor $\cos^2 i$ in the left-hand side of (1) to account for the disc inclination, where i is the angle between the normal to the plane of the disc and the direction of motion of the galaxy through the ICM. We have chosen to neglect this factor because studies based on SPH simulations agree that the galaxy inclination does not have a significant influence on the amount of removed gas; strong RPs that strip a face-on galaxy also strip a galaxy moving edge-on, although on a slightly longer time-scale (see Roediger 2009, and references therein). We have also chosen to ignore the possibility of enhanced star formation as a result of RP compressing the molecular gas of the galaxy (Fujita & Nagashima 1999; Bekki & Couch 2003; Kronberger et al. 2008; Kapferer et al. 2009), since observational evidence is contradictory (Koopmann et al. 2006; Koopmann & Kenney 2006; Abramson & Kenney 2009) and theoretical work needs confirmation due to the complex nature of star formation.

In SAG the evolution of the galaxy population is followed by solving differential equations describing the physical processes involved, such as gas cooling, star formation and feedback, at small time-steps of size $\Delta T/N_{\rm steps}$, where ΔT is the time interval between outputs of the underlying cluster simulation; we adopt $N_{\rm steps} = 50$. Since the hydrodynamical properties of the ICM and galaxy positions and velocities are given by the underlying simulation, the effect of RPS is estimated for each galaxy only once per snapshot, considering a single instantaneous stripping event and assuming that the profile of the exponential disc remains unaltered for $R < R_{\rm str}$. The mass of gas removed by RPS is transferred to the hot gas component of the central galaxy of its FOF halo, thus becoming available to the central galaxy for cooling and star formation in subsequent time-steps.

The RPS effect eats away the gas disc from the outside in. After the first stripping event, the remaining disc gas (if any is left) is assumed to form an exponential disc with the same scalelength as before the stripping, but sharply truncated at $R_{\rm str}$. If in a subsequent snapshot the galaxy experiences a higher RP, $R_{\rm str}$ will then be smaller and the gas lost to RPS will be the gas located between $R_{\rm str}(t_n)$ and $R_{\rm str}(t_{n-1})$, where t_n and t_{n-1} denote the current and previous simulation outputs, respectively. Since in our strangulation model satellite galaxies have no infall of cooling gas, their gaseous discs cannot be re-built. It is also unlikely that the remaining disc gas would systematically gain angular momentum so as to regenerate a full exponential disc. With these considerations, if $R_{\rm str}(t_n) < R_{\rm str}(t_{n-1})$, the mass of cold gas removed by RPS at time t_n can be shown to be

$$M_{\rm RP}(t_n) = M_{\rm cold}(t_n)\frac{f_s(t_n) - f_s(t_{n-1})}{1 - f_s(t_{n-1})}, \tag{10}$$

where $M_{\rm cold}(t_n)$ is the mass of cold gas in the galactic disc at the current snapshot but before RPS acts, and f_s is given by

$$f_s(t) = \left(1 + \frac{R_{\rm str}(t)}{R_{\rm d}}\right)\exp\left(-R_{\rm str}(t)/R_{\rm d}\right). \tag{11}$$

This takes into account that if all the cold gas mass is between $R = 0$ and $R = R_{\rm str}$ in the form of a truncated exponential disc, then the expression (2) for the central surface density of the cold gas becomes

$$\Sigma_{0,\rm cold}(t_n) = \frac{M_{\rm cold}(t_n)}{2\pi\left[1 - f_s(t_{n-1})\right] R_{\rm d}^2}. \tag{12}$$

Conversely, if in a subsequent snapshot the galaxy experiences a lower RP, $R_{\rm str}(t_n)$ will be larger than the radius at which the remaining gas is found, $R_{\rm str}(t_{n-1})$. In such a case, we set $R_{\rm str}(t_n) = R_{\rm str}(t_{n-1})$ and no gas is removed in that time-step.

In addition to RPS, gas could be removed from the galaxy by turbulent stripping, caused by the generation of Kelvin–Helmholtz and/or Rayleigh–Taylor instabilities at the interface between the cold gas and the ICM. However, we do not consider this possibility as the time-scale associated with the growth of such instabilities is generally much longer than the RPS time-scale, as shown by McCarthy et al. (2008) in their work (see also Font et al. 2008).

Finally, we would like to emphasize once again that RP is calculated for every satellite galaxy in the entire simulation. We do not restrict the calculation to galaxies residing within the most massive groups, and we do not turn on the calculation at a selected redshift; RP will act on galaxies whenever condition (1) is satisfied.

4 RESULTS

4.1 Radial profiles and distributions of RP

The procedure outlined in the previous section allows us to follow the evolution of the properties of the intergalactic medium within DM haloes, obtaining for each snapshot values of the ambient density and relative velocity for each satellite galaxy. In this section we discuss the distributions and radial profiles of RP that we obtain for satellites in the simulated clusters, and their evolution with time.

An interesting point is to evaluate how our RP model compares with previous studies which assume analytic density profiles for the ICM (Okamoto & Nagashima 2003; Lanzoni et al. 2005; BDL08). Hence, additionally, we estimate the RP and the properties of galaxies assuming that the ICM gas is in hydrostatic equilibrium following a NFW profile, re-scaled according to the adopted baryonic fraction. These profiles are calculated using the concentration parameter determined for the cluster at each redshift. We will refer to this as the 'analytic' method, and to our new implementation described in Section 3.1 as the 'gas-particles' method.

The dependence on clustercentric distance of the ICM density, relative velocity (squared) of the satellites with respect to the ICM and the resulting RP is plotted in Fig. 2 for three different redshifts, where we show the results obtained for one of the G15 clusters (taking into account the properties of the main cluster progenitor when considering redshifts $z > 0$). In all other clusters we find a similar behaviour, so we choose this one as representative of the general trends. The median values obtained with the gas-particles method are shown with black points, and shaded areas mark the regions enclosed by the 5th and 95th percentiles of the distributions. In these plots we include all galaxies identified as satellites belonging to the cluster FOF halo at each selected redshift, and the ICM properties are sampled at the positions of the galaxies.

The top panels of Fig. 2 show the ICM density profiles obtained. As the cluster grows in mass from $\log(M_{\rm vir}/h^{-1}\,{\rm M}_{\odot}) \simeq 13.7$ up to 15.1 between $z = 2$ and 0, the median density in the cluster central region ($r < 0.5r_{\rm vir}$) increases about one order of magnitude. At the virial radius, the increase between $z = 1$ and 0 is smaller. The median density profile decreases monotonically at the present epoch over four orders of magnitude, in the range $0 < r/r_{\rm vir} < 2$. We compare these results with the ICM profiles determined for the analytic method (shown with dotted lines in the top panels of Fig. 2). The match between the median density profile determined from the simulation and the NFW analytic profile is excellent at $z = 0$; however, for $z \geq 1$, NFW profiles tend to overestimate (underestimate) the density for $r < r_{\rm vir}$ ($r > 1.5r_{\rm vir}$).

The median square velocities of the satellite galaxies relative to the ICM are shown in the middle panels of Fig. 2. The velocity distribution of cluster galaxies is already established at $z \simeq 1$ (at least for $r < 1.5r_{\rm vir}$), as can be seen from the similarities between the radial profiles at both $z = 1$ and 0. There is a trend of increasing median relative velocity for decreasing radius, with a large scatter at all radii. At $z = 2$, the velocity profile is flatter and the median velocities are lower than for $z \leq 1$.

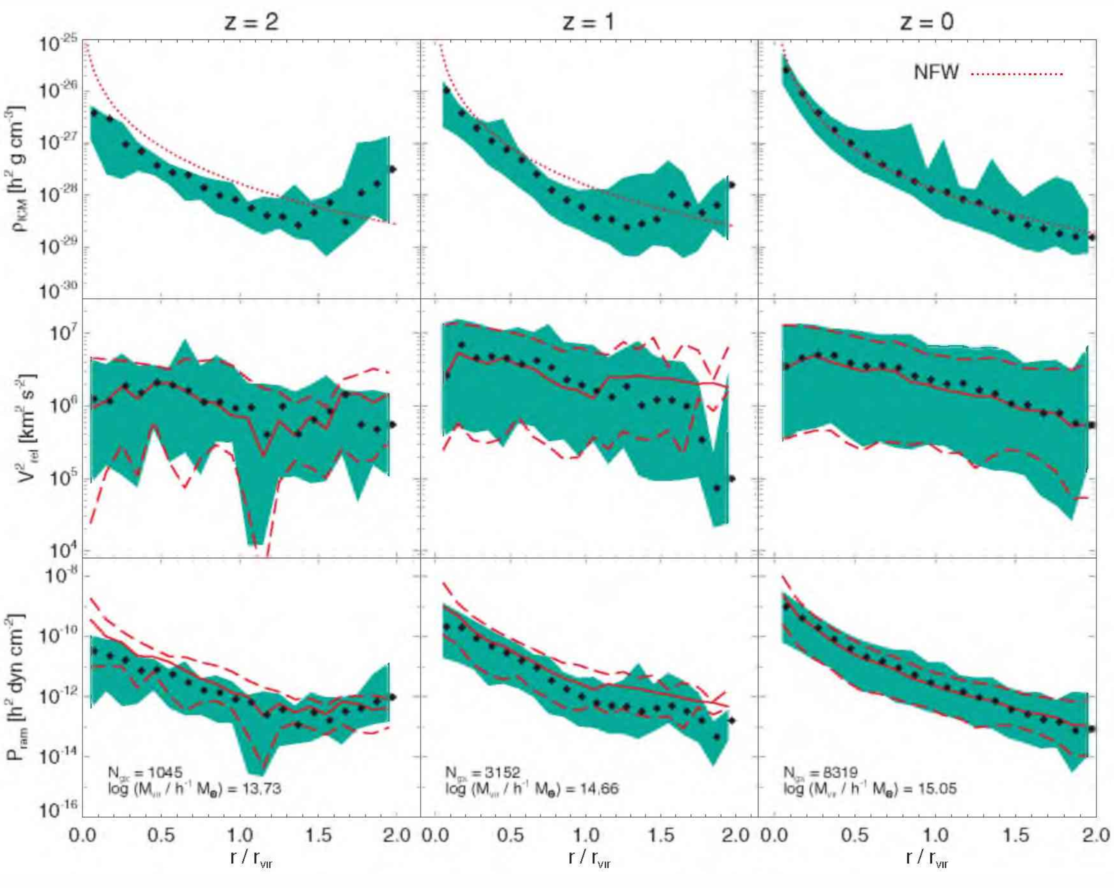

Figure 2. Values of ICM density (top), galaxy velocity relative to the ICM (centre) and RP (bottom) as a function of the distance to the cluster centre, at the current positions of all satellite galaxies identified as members of the FOF group corresponding to one of the G15 clusters. Results are shown for three different redshifts: $z = 2$ (left), $z = 1$ (centre) and $z = 0$ (right). Diamonds indicate median values in bins of $0.1r/r_{\rm vir}$, and the shaded areas mark the regions enclosed by the 5th and 95th percentiles in each bin. The dotted line in the top panels is a NFW density profile with the concentration c of the halo at that redshift. The solid line in the middle panels indicates the median velocity of the galaxies in the rest frame of the cluster, and the dashed lines enclose the 5th and 95th percentiles of that distribution. In the bottom panels, the solid line indicates the median RP obtained by multiplying the density given by the NFW profile by the rest-frame velocity; dashed lines denote the 5th and 95th percentiles.

On any given cluster, the evolution of the RP experienced by satellite galaxies for $z \leq 1$ depends mainly on the build-up of the ICM density over time, as the cluster velocity profile is already established at $z \simeq 1$. The bottom panels of Fig. 2 show that RP increases approximately one order of magnitude at the cluster centre between $z = 1$ and 0, consistent with the increase in ICM density. Following the trend set by the density, the RP stays at roughly the same level for $1 < r/r_{\rm vir} < 1.5$ between $z = 2$ and 1, and increases slightly between $z = 1$ and 0. For $r > 1.5r_{\rm vir}$, the median RP seems to drop between $z = 2$ and 1, and stays roughly similar for $z \leq 1$. This happens because, in this region, the median density decreases over time but the mean relative velocity of galaxies increases, thus resulting in similar RP values.

To determine the RP in the analytic method we also need an estimation of the relative velocities of galaxies. If these are not determined using the gas particles in the simulations, the alternatives are either to draw them at random from an assumed distribution (Lanzoni et al. 2005) or to take the velocity of the satellite (as given by the semi-analytic model) in the rest frame of its central galaxy (BDL08). If the ICM is hydrostatic this latter approach should be a good approximation, and this is what we use for the analytic method. The results of this are shown with lines in the middle panels of Fig. 2. The agreement between the analytic and gas-particles methods is again excellent at $z = 0$, and also at $z = 1$ for $r \lesssim r_{\rm vir}$, for both the median (solid line) and the scatter (dashed lines). At $z = 1$, rest-frame velocities tend to be larger for $r > r_{\rm vir}$ than the velocities relative to the gas particles.

The analytical distribution of RP that results of multiplying the median density given by the NFW profile by the square of the rest-frame velocities is shown with lines in the bottom panels of Fig. 2. As expected from the very good agreement between both approaches, both for the density and the relative velocity at $z = 0$, the RP profiles are very similar at the present epoch. The agreement is not so good for $z \geq 1$ where the shape of the RP profiles are similar but in the analytical model the mean values and the levels of the percentiles shift to higher values. According to the results of our self-consistent numerical approach, the analytic method appears to overestimate the RP over most of the range considered.

To quantify this latter point, in Fig. 3 we plot the average difference between the RP determined from the gas-particles and the analytic methods, normalized to the analytical value of RP. Results are shown in different colours for $z = 2$, 1, 0.5 and 0. The left-hand panel shows the result of averaging over all the simulated clusters, and error bars show the 1σ cluster-to-cluster scatter. From this plot we can clearly see that the analytic method always overestimates the value of RP for $r \lesssim 1.5r_{\rm vir}$ (although at $z = 0$ and for $r \gtrsim 0.4r_{\rm vir}$ it could be said that both models agree within the errors). The difference between the two models increases with redshift; this trend is clear within $r_{\rm vir}$, but becomes noisier outside of it (perhaps due to the smaller number of cluster galaxies in these regions). These trends persist if we consider separately the G14 and G15 clusters (middle and right-hand panels in Fig. 3, respectively).

The distribution of RP values experienced by satellite galaxies within $r_{\rm vir}$ in our simulated clusters is shown in Fig. 4 for the G14 clusters (top) and G15 clusters (bottom) at redshifts $z = 1$ (left) and $z = 0$ (right). We compare results obtained from the gas-particles method (histograms in black lines) and the analytic method (histograms with dashed lines). All the distributions can be well fitted by Gaussian functions, and the result of the fits we obtained for these histograms is shown in Table 1. The mean value of RP obtained from both the gas-particles and analytic methods are higher for the more massive clusters, a feature that is also present at higher redshifts. We mentioned before that for a given cluster the increase of RP for $z \lesssim 1$ is due to the increase in ICM density, but the difference between the RP values for different cluster masses is due to a combination of increased density and relative velocity. On average, the ICM density within $r_{\rm vir}$ in G14 clusters can be as high as 75 per cent of the density at same radii in G15 clusters. The rest of the difference is due to the lower relative velocity of satellites in the smaller clusters (within $r_{\rm vir}$, the mean velocity in G14 clusters is ∼25 per cent of the mean v in G15 clusters).

The range of RP values we obtain at $z = 0$ for both models is similar to that found by BDL08, who calculate values of RP for clusters of masses comparable to ours, extracted from the De Lucia & Blaizot (2007) semi-analytic catalogue. BDL08 assume an ICM described either by an isothermal or a Komatsu & Seljak (2001,

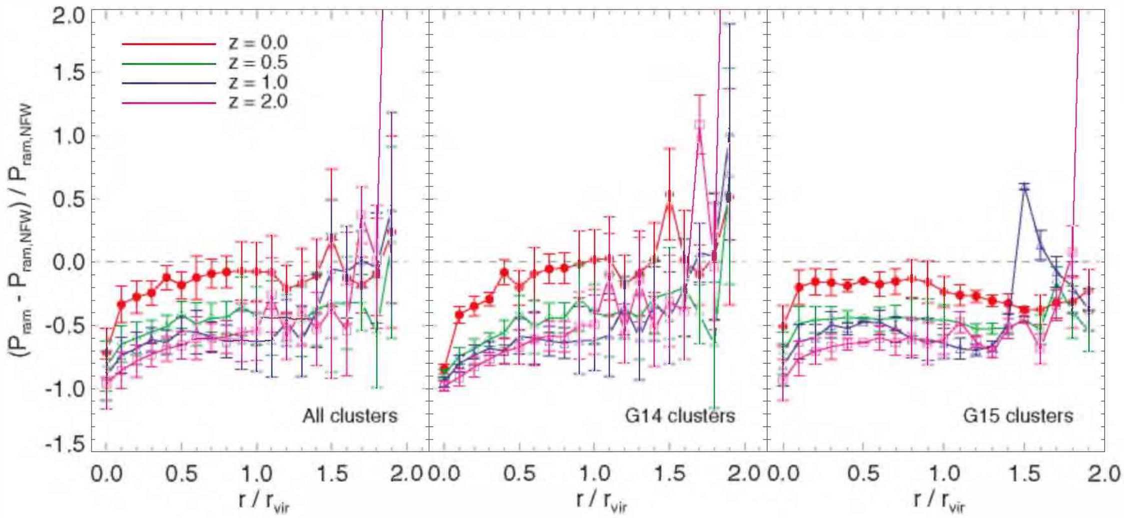

Figure 3. Average difference between the RP determined from the gas particles in the simulation and the RP calculated as the product of a NFW density profile and the squared velocities of the satellite galaxies in the rest frame of the clusters. Results are shown for $z = 2$, 1, 0.5 and 0, and for all the simulated clusters (left), the G14 clusters only (centre) and the G15 clusters only (right).

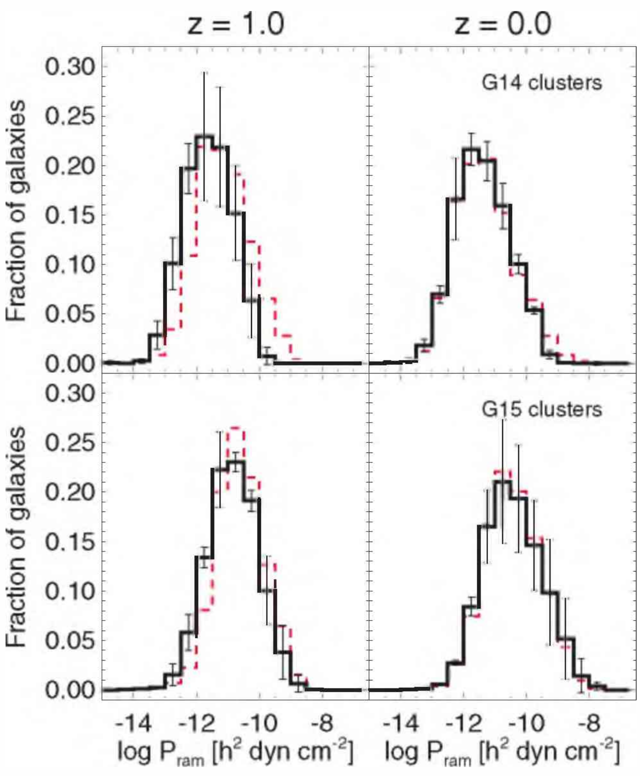

Figure 4. Histograms of the RP experienced by the galaxies within $r_{\rm vir}$ in the simulated clusters at $z = 1$ (left) and $z = 0$ (right), obtained from the gas-particles method (black lines) and the analytic method (dashed lines). Results for the G14 and G15 clusters are shown in the top and bottom panels, respectively. Error bars denote the 1σ cluster-to-cluster scatter and for clarity are shown only for the gas-particles method.

hereafter KS01) model, in hydrostatical equilibrium within a NFW halo. For the case of the isothermal model, BDL08's distribution of RP is fairly skewed, with a sharp cut-off at higher pressures; for the KS01 model they obtain a much more symmetrical distribution (see their figs 1 and 2, respectively). Comparing the shapes of our local RP distributions, given in the right-hand panels of Fig. 4, with those of BDL08, we find better agreement with their results for the KS01 model. The local mean RP values obtained from our gas-particles method (see Table 1) are also in good agreement with those determined by BDL08 with the KS01 model, who find $10^{-11.3}$ dyn cm^{-2} for their set of 10^{14} M$_\odot$ clusters, and $10^{-10.7}$ dyn cm^{-2} for their 10^{15} M$_\odot$ clusters.

As already noticed from Fig. 2, we can see again in Fig. 4 that the distributions obtained with both methods agree very well at the present epoch, but not so for higher redshifts. For both sets of clusters, the mean value of RP obtained from the gas-particles method for galaxies within the virial radius increases approximately half an order of magnitude from $z = 1$ to the present. However, in the analytical calculation, the mean values at both redshifts are much more similar (in the case of the G14 clusters, if errors are taken into account then the mean values can be considered equal). This fact, combined with the results shown in Fig. 3, indicates that the RP in the clusters does not grow over time in the same way in both models.

To better visualize this, we plot in Fig. 5 the mean RP for galaxies within $r_{\rm vir}$ as a function of redshift, for both sets of clusters. Mean RP values given by the gas-particles method are shown with black symbols, and the shaded areas indicate the regions within 1σ of the mean. Solid lines indicate the mean values obtained from the analytical calculation, with dashed lines enclosing the regions within 1σ of the mean. For both models, the difference between the mean RP values of both cluster sets at a given z is always about one order of magnitude, being larger in the more massive clusters, as expected.

In the simulations by Roediger & Brüggen (2006), values of RP of order 10^{-12} dyn cm^{-2} were called weak, 10^{-11} dyn cm^{-2} medium and 10^{-10} dyn cm^{-2} strong. Roediger & Brüggen (2006) find that a spiral galaxy with mass $\sim 2 \times 10^{11}$ M$_\odot$ subject to strong RP will typically lose all of its gas within ~50 Myr, medium RP will remove approximately half of the gas within ~200 Myr and weak RP removes relatively small amount of gas (the actual gas loss will depend on the structure of the gaseous, stellar and DM components). Fig. 5 shows that for the gas-particles model the majority of satellite galaxies in the massive G15 clusters are experiencing medium level RP already at $z \sim 2$, and at $z \lesssim 0.5$ about 20 per cent of satellites experience strong levels of RP at any given time. In the case of the G14 clusters, the mean RP is between medium and weak for $z \lesssim 1.5$, and few galaxies ever experience strong levels of RP; only at $z \sim 1$ does a significant fraction of satellites begin to experience medium levels of RP.

In the analytic model, at higher redshifts ($z \gtrsim 1$), the mean RP for the G15 clusters reaches medium values and a significant fraction of satellite galaxies already experience medium-to-strong levels of RP at $z \sim 2$. A similar situation occurs for the G14 clusters, with the values of RP shifted to the range of weak-to-medium levels, the difference between the two models being larger for higher redshifts. In both models the scatter around the mean is large, spanning one order of magnitude at each side of the mean. The dispersion in the distributions also grows slightly with time, as can be better appreciated from Table 1, where we can see an increase in σ of about 10 per cent between $z = 1$ and 0, for both sets of clusters. This may arise as a result of the larger number of galaxies in clusters at the present time (about three times more galaxies than at $z = 1$).

Although the results for both models agree at $z \sim 0$ for the different sets of clusters, the different evolution of RP over time is clear. While the mean RP values obtained from gas-particles

Table 1. Best-fitting parameters of Gaussian functions to the RP histograms of Fig. 4. $\langle \log P_{\rm ram} \rangle$ and $\sigma_{\rm ram}$ denote the mean and dispersion of each distribution, respectively.

z	G14 clusters $\langle \log P_{\rm ram} \rangle$ (h^2 dyn cm^{-2})	G14 clusters $\sigma_{\rm ram}$	G15 clusters $\langle \log P_{\rm ram} \rangle$ (h^2 dyn cm^{-2})	G15 clusters $\sigma_{\rm ram}$	Model
1.0	-11.64 ± 0.08	0.73 ± 0.05	-10.91 ± 0.03	0.76 ± 0.02	Gas-particles
	-11.14 ± 0.07	0.84 ± 0.05	-10.63 ± 0.05	0.75 ± 0.03	Analytic
0.0	-11.33 ± 0.03	0.87 ± 0.02	-10.51 ± 0.09	0.83 ± 0.04	Gas-particles
	-11.18 ± 0.05	0.96 ± 0.03	-10.47 ± 0.07	0.81 ± 0.03	Analytic

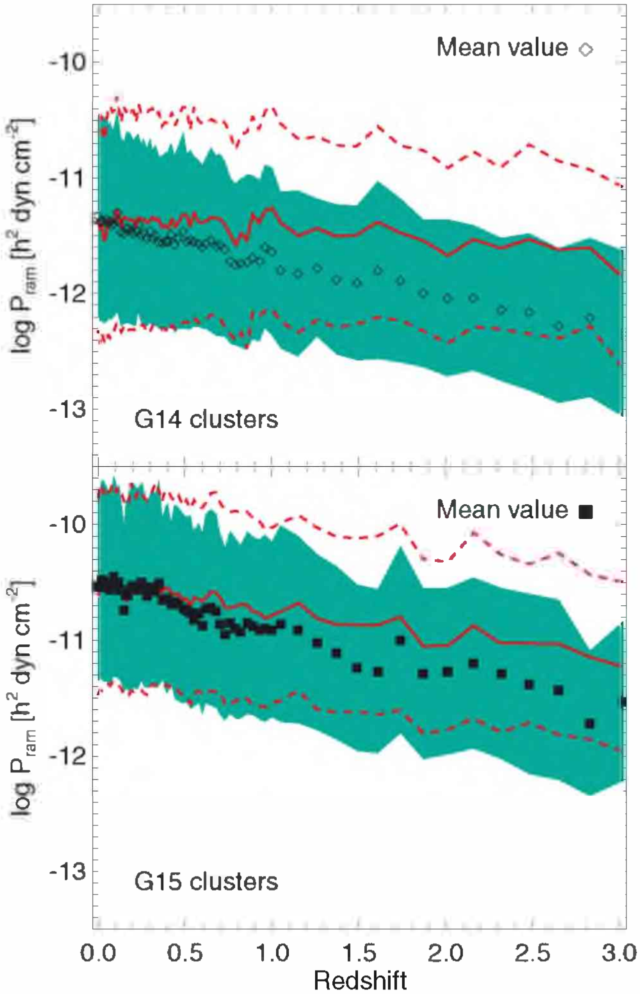

Figure 5. Mean RP exerted on the galaxies within $r_{\rm vir}$ of the simulated clusters as a function of redshift. Top and bottom panels show results for the G14 and G15 clusters, respectively. Open diamonds and filled squares indicate the mean value of RP for the gas-particles method and the shaded areas denote the regions within 1σ of the mean. Solid lines indicate the mean RP for the analytic method, and the dashed lines enclose the region within 1σ of the mean.

method increase almost exponentially with redshift, the evolution of the mean RP in the analytic method is flatter, especially so in the case of the G14 clusters. The lack of strong evolution of the mean RP values for G14 clusters is a consequence of the overestimation of RP by the analytic model for the inner parts of the clusters ($r < 0.5r_{\rm vir}$), even at $z \sim 0$ (see middle panel of Fig. 3). This is because these clusters, and their progenitors at higher redshift, are galaxy group-sized systems of virial masses in the range $\sim10^{13}$–$10^{14}\,h^{-1}\,{\rm M}_{\odot}$, whose ICM distributions are not so well described by a NFW profile. There is also a clear but smaller difference between the models for the case of the G15 clusters. For $z \lesssim 0.5$, both models agree fairly well; this can be due to the fact that these clusters are already massive systems at $z \sim 2$, and so their ICM is better described by a NFW profile (see radial profiles for different cluster masses in the top panels of Fig. 2).

In Fig. 6 we plot RP histories given by our gas-particles method for randomly selected satellite galaxies of type 1 (black dot-dashed lines) and type 2 (black solid lines). Results are shown for one of the G15 clusters (left) and one of the G14 clusters (centre). For comparison, the right-hand panel of Fig. 6 shows the RP evolution for galaxies within one halo with virial mass $\simeq10^{13}\,h^{-1}\,{\rm M}_{\odot}$ extracted from the simulation box of one of the G15 clusters. There are differences between the RP histories of different types of satellites. For type 2 satellites, the RP typically oscillates, increasing on average; whereas for type 1 galaxies, the typical history is one of monotonically increasing RP. This difference in the RP histories is due to the way in which positions and velocities of galaxies are assigned in the code, being more reliable for type 1 galaxies. As mentioned in Section 2.2 the position and velocity of a galaxy are assigned by tracking the most-bound DM particle of its host DM subhalo. In the case of type 1 galaxies this subhalo still exists and is affected by dynamical friction, but for type 2 galaxies it has been destroyed by tidal forces and we are then tracking a single DM particle. The regions enclosed by the maximum and minimum RP values reached by all the galaxies that are present at $z = 0$ in the selected halo are depicted by dashed lines and shaded areas for the analytic and gas-particles methods, respectively. Once again, we see differences between the models; satellites in the analytical model reach higher values of RP in all three cases, and the difference between both methods increases with decreasing halo mass.

4.2 Effects of ram pressure stripping

After analysing the evolution of the distributions of RP values and the dependence on the cluster mass obtained from two different models, we now focus on the values given by the gas-particles method and explore the influence of RPS on galaxy properties. The new estimation of the size of galactic discs, described in Section 3.2, affects the results of the disc instability process implemented in SAG. This calls for a retuning of the free parameters of SAG in order to retain a good fit to observed properties such as the b_J- and K-band cluster luminosity functions and the BH–bulge mass relation, among others. Three parameters change with respect to those used by LCP08 (see the descriptions of the model parameters in LCP08). Specifically, the parameters $\kappa_{\rm AGN}$ and $f_{\rm BH}$, which control the rate of gas accretion on to the central BH, increase from 2.5×10^{-4} to $10^{-3}\,{\rm M}_{\odot}\,{\rm yr}^{-1}$, and from 0.015 to 0.04, respectively; the disc instability threshold $\epsilon_{\rm disc}$ decreases from 1.1 to 0.85. This recalibration is done without considering RPS. We then run three sets of models: one without and two with RPS, using the same set of parameters in all cases in order to evaluate the effect of RPS on galaxy properties. In the following, we will use SAG to refer to the semi-analytic model without RPS, and SAGRP and SAGRP-A will denote the models where RP values are determined using the gas-particles or the analytical methods, respectively.

As a test of the performance of the model, Fig. 7 shows the stripping radius of disc satellite galaxies for the SAGRP model as a function of the peak RP that they experience. Results for the mean stripping radius and 1σ scatter are plotted for disc satellite galaxies in two different mass ranges: $10^{10} \le M_{\rm stellar} < 7 \times 10^{10}\,h^{-1}\,{\rm M}_{\odot}$ (dot–dashed lines) and $7 \times 10^{10} \le M_{\rm stellar} < 2 \times 10^{11}\,h^{-1}\,{\rm M}_{\odot}$ (solid lines). We compare this with the results of several N-body/hydrodynamical simulations specially focused on the study of RPS in individual galaxies (denoted by different symbols). These simulations employ different procedures to compute the hydrodynamics (SPH: Abadi et al. 1999; Schulz & Struck 2001; Jáchym et al. 2007; Eulerian: Quilis et al. 2000; Roediger & Hensler 2005; sticky particles: Vollmer et al. 2001). All the simulations consider Milky Way-class galaxies entering a dense environment, except for Schulz & Struck (2001) who study a smaller galaxy with $M_{\rm stellar} \simeq 6 \times 10^{10}\,h^{-1}\,{\rm M}_{\odot}$. Jáchym et al. (2007) run simulations for different

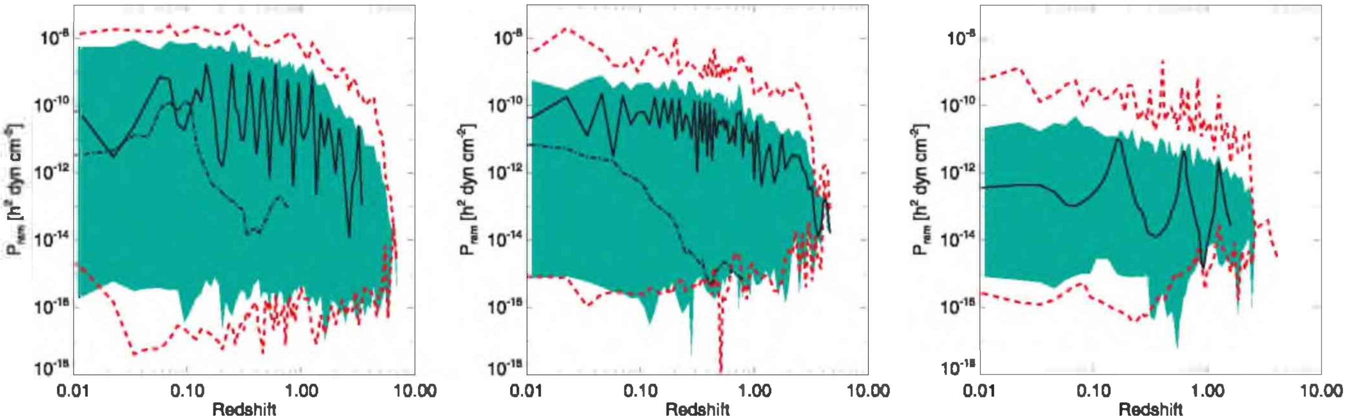

Figure 6. RP histories of satellite galaxies in one of the G15 clusters (left), one of the G14 clusters (centre) and in one group with $M_{\rm vir} \simeq 10^{13}\,h^{-1}\,{\rm M}_{\odot}$ (right) which is contained in the simulation box of one of the G15 clusters. Solid black lines correspond to a selected type 2 satellite, and black dot-dashed lines to a type 1 satellite. Shaded areas mark the regions enclosed by the maximum and minimum RP reached by all the galaxies present in the cluster at $z = 0$ as determined from the gas-particles method; dashed thick lines denote the maximum and minimum values of the RP calculated with the analytic method.

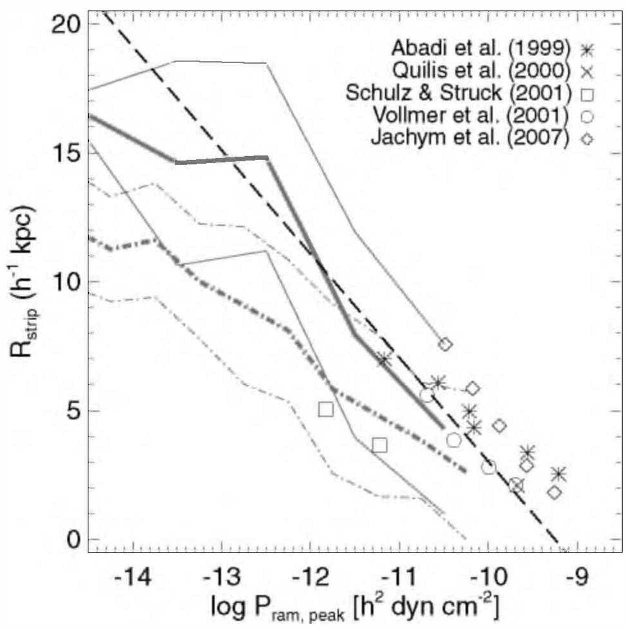

Figure 7. Stripping radius $R_{\rm str}$ as a function of the peak RP experienced by disc satellite galaxies ($M_{\rm bulge}/M_{\rm stellar} \leq 0.95$). Thick dot–dashed and solid lines denote the mean $R_{\rm str}$ for satellites with $10^{10} \leq M_{\rm stellar} < 7 \times 10^{10}\,h^{-1}\,{\rm M}_{\odot}$ and with $7 \times 10^{10} \leq M_{\rm stellar} < 2 \times 10^{11}\,h^{-1}\,{\rm M}_{\odot}$, respectively, and thinner lines enclose the regions within 1σ of the mean values. Points show the results of different N-body/hydrodynamical simulations of RPS in single galaxies. The dashed line shows the analytical estimate of equation (9) for a Milky Way-class galaxy, with surface densities of stars and gas taken from Flynn et al. (2006).

types of clusters; here we select the results for their standard cluster model. The dashed line shows the analytical estimate for $R_{\rm str}$ of equation (9) for a Milky Way-like galaxy, with surface densities for stars and gas taken from Flynn et al. (2006). There is a good agreement between the GG72 estimate and the different simulations (for clarity we do not plot the results from Roediger & Hensler 2005, as they are very similar to the GG72 line).

Even though a comparison between our method and the detailed simulations is not direct, since the initial conditions are not necessarily the same, the general trend seen in the detailed simulations is reproduced in our model for galaxies of similar stellar masses. We note that the comparison does not include those satellite galaxies from our simulations whose cold gas is completely stripped ($R_{\rm str} = 0$). There are no such galaxies for $\log P_{\rm ram,peak} \lesssim -11.5$, and the majority of fully stripped galaxies ($\gtrsim 80$ per cent) are found at $\log P_{\rm ram,peak} \gtrsim -10.5$.

One of the galaxy properties most directly affected by RPS is the cold gas content. Fig. 8 shows the fraction of galaxies that have lost all of their cold gas ($f_{\rm no-gas}$) as a function of clustercentric distance, for G14 and G15 clusters. To construct this plot, we select galaxies within $2r_{\rm vir}$ of the simulated clusters and with stellar mass $\geq 10^9\,h^{-1}\,{\rm M}_{\odot}$. For this plot all galaxies within $r_{\rm vir}$ are considered, not only members of the main FOF group; so we are including members of outlying groups which are infalling into the main cluster. The fractions of gas-depleted galaxies are determined for the three different semi-analytic models considered, which are represented by different line types. Different colours identify the redshifts at which results are shown. For the SAG model, $f_{\rm no-gas}$ is very low; only in the innermost regions ($r \lesssim 0.2r_{\rm vir}$) the gas fractions increase from $f_{\rm no-gas} \approx 0.2$ to 0.3 in the redshift interval $1 < z < 0$, regardless of cluster mass. These galaxies are those that have spent enough time within the cluster to gradually consume their cold gas reservoir; recall that cooling flows are suppressed in satellite galaxies due to strangulation. In SAG, $f_{\rm no-gas}$ has an almost flat radial distribution beyond $0.5r_{\rm vir}$ (dashed lines in Fig. 8).

When RPS is acting, almost all galaxies in the innermost regions of clusters lose their cold gas by $z = 0$, for both sets of clusters. The fractions of gas-depleted galaxies in the SAGRP model decrease for larger distances to the cluster centre, but they remain significant at $r \simeq 2r_{\rm vir}$, being larger for G15 clusters ($f_{\rm no-gas} \simeq 0.5$) than for G14 ones ($f_{\rm no-gas} \simeq 0.3$). The lower values of $f_{\rm no-gas}$ in the outskirts of G14 clusters in the models that include RPS are also consistent with the weak-to-medium values that RP takes in these clusters. This monotonic decrease of $f_{\rm no-gas}$ with clustercentric distance is a direct consequence of the behaviour of the radial profile followed by RP values (see bottom panels of Fig. 2).

The evolution of the cold gas content of galaxies in the SAG model is very similar for clusters of different masses; however, this is not the case for galaxies in models which include RPS. The difference of over half an order of magnitude between the mean RP values for G14 and G15 clusters at different redshifts, which is clearly visible in Fig. 5, drives a rather different evolution of the fraction of galaxies devoid of cold gas. In the SAGRP model, for G15 clusters

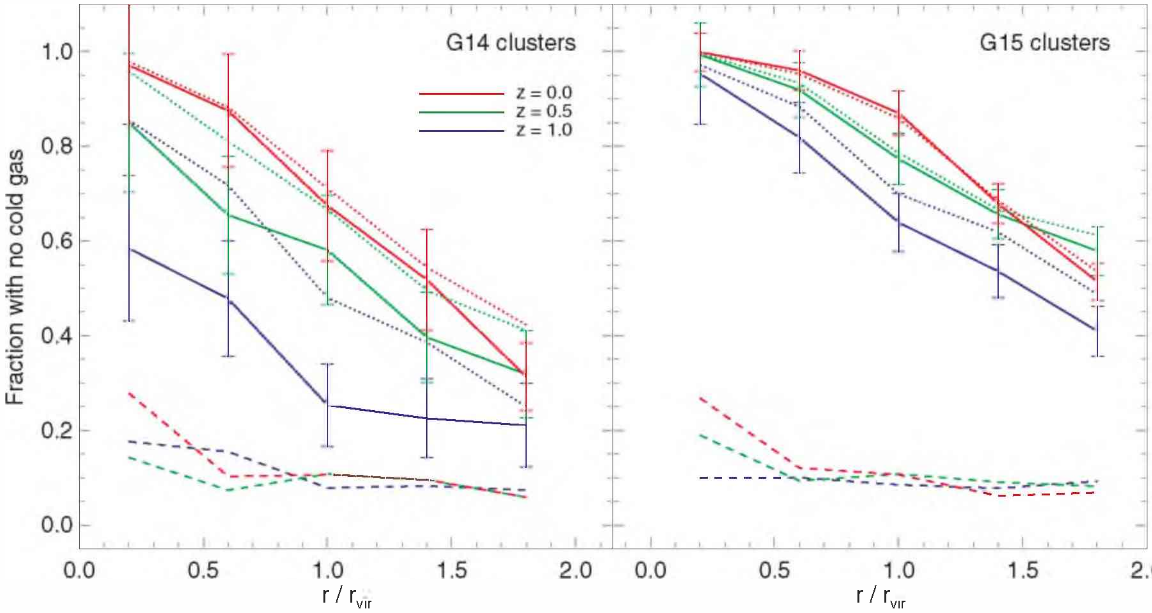

Figure 8. Fractions of galaxies that have lost all of their cold gas as a function of distance to the cluster centre, for G14 clusters (left) and G15 clusters (right). Results are shown for three different redshifts: $z = 1$, 0.5 and 0, and for three models: SAG (dashed lines), SAGRP (solid lines), which takes into account RP values estimated from the gas-particles method, and SAGRP-A (dotted lines), where the RP is calculated with the analytic method. All galaxies within $2r_{\rm vir}$ of the simulated clusters and with stellar mass greater than $10^9\,h^{-1}\,{\rm M}_{\odot}$ are included in this plot. Galaxies are binned in $0.4r/r_{\rm vir}$, and error bars are only shown on the SAGRP model for clarity.

the situation at $z = 0$ regarding the cold gas content of galaxies has been practically established at $z = 0.5$, and it does not evolve much since $z = 1$. Although at this latter redshift the fractions are ≈10–20 per cent lower than at $z = 0$ at all radii, they are quite high ($f_{\rm no-gas} \gtrsim 0.5$) even in the cluster outskirts. Conversely, for the case of the G14 clusters we see a stronger evolution in the fractions of gas-depleted galaxies in the same redshift interval. This reflects a more gradual removal of the cold gas of satellites as a result of the lower values of RP in these clusters. In the outskirts of the G14 clusters $f_{\rm no-gas} \sim 0.3$, lower than for G15 clusters but still much larger than in the SAG model.

The results described above clearly show a dependence of the evolution of the fraction of gas-depleted galaxies on cluster mass. This trend is different for the analytic estimation of RP used in the SAGRP-A model, shown by dotted lines in Fig. 8. Both for the G14 and G15 clusters, the final values of $f_{\rm no-gas}$ are reached at higher redshift than for the SAGRP model. For instance, in the case of the G14 clusters, the value of $f_{\rm no-gas}$ in the SAGRP-A model at $z = 1$ is already as high as the value reached for the SAGRP model at $z = 0.5$. This behaviour is the result of the much higher values of RP at $z > 0$ in the SAGRP-A model (see Fig. 5).

In the models that include RPS, the higher fractions of gas-depleted galaxies found at $z = 0$ in the cluster outskirts, for both sets of clusters, indicate that during cluster assembly RPS has an important effect on the galaxies contained in the smaller subgroups that are being accreted by the cluster; this is what has been called 'pre-processing' (e.g. Fujita 2004; Mihos 2004). This idea is also inferred from observational evidence of compact group of galaxies falling into the massive galaxy clusters Abell 1689 ($z \sim 0.18$), Abell 2667 ($z \sim 0.23$) and Abell 1367 ($z \sim 0.02$) (Cortese et al. 2006, 2007); galaxies within these groups show extended tails of ionized gas, that can be interpreted as the signature of RPS. We then find that RPS is a process that significantly affects the cold gas content of galaxies and the rate at which it is removed, which depends on cluster mass. Consequently, the RPS experienced by satellite galaxies might enhance differences in the star formation history and the colour evolution on haloes of different masses; this will be explored in detail in a forthcoming paper.

5 CONCLUSIONS

We develop a new method to describe the effects of RPS on galaxy properties which works within the SAG semi-analytic model of galaxy formation and evolution, in combination with cosmological hydrodynamical N-body/SPH simulations of galaxy clusters. RPS is implemented in SAG adopting the GG72 criterion. The novel feature of our implementation is that the kinematical and thermodynamical properties of the hot gas responsible for RP are obtained from the gas particles of the SPH simulations (gas-particles method). This results in a more self-consistent estimation of the RP experienced by satellite galaxies.

We compare our results with those obtained from an analytic estimation of RP, which considers a NFW density profile for the hot gas contained within DM haloes, re-scaled according to the adopted baryonic fraction (analytic method). We analyse the dependence on clustercentric distance and redshift of the RP values given by both methods, and evaluate the influence of the environment on the behaviour of these distributions. The RPS method discussed in this work can be adapted to work with any kind of cosmological simulation that includes gas physics, regardless of the particular numerical scheme used for the hydrodynamical calculations. However, the specific results from its application might depend on the details of the numerical implementation. For example, the SPH method utilizes an artificial viscosity term to properly capture hydrodynamic shocks, and this viscosity can artificially suppress turbulence in the ICM (Dolag et al. 2005; Agertz et al. 2007). The simulations we have used include the standard SPH artificial viscosity. The use of a lower viscosity formulation of SPH, or a grid-based method, may result in an increased level of ICM turbulence. This could result in the distribution of the velocities of galaxies relative to the gas deviating further from the velocities calculated by assuming a hydrostatic ICM.

We have selected from the simulations considered two sets of cluster-sized haloes, with masses $M_{\rm vir} \simeq 10^{14}\,h^{-1}\,{\rm M}_{\odot}$ (G14 clusters) and $M_{\rm vir} \simeq 10^{15}\,h^{-1}\,{\rm M}_{\odot}$ (G15 clusters). The RP values obtained by the gas-particles and analytic methods are used by the RPS process implemented in the semi-analytic model, resulting in the models SAGRP and SAGRP-A, respectively. These models provide a galaxy population affected by RPS; their results are compared with those obtained from the standard SAG, which does not take RPS into account, in order to evaluate the effect of RPS on the cold gas content. We summarize our main results.

(i) The RP estimated from the gas-particles method increases approximately one order of magnitude at the cluster centre between $z = 1$ and 0, consistent with the increase in ICM density, since the cluster velocity profile is already established at $z = 1$. Median RP values do not evolve much in the outskirts of the cluster ($r/r_{\rm vir} > 1$), which is a consequence of the combined behaviour of the median ICM density and the relative velocities, whose radial distributions decrease and increase with time, respectively.

(ii) The radial distributions of median ICM density, velocity relative to the ICM and RP in the gas-particles method follow smooth profiles at $z = 0$, and these distributions are very well traced by analytical estimations based on NFW profiles for the ICM density. However, the agreement is not so good for $z \geq 1$, where the shape of the RP profiles are similar but the mean values and levels of the percentiles shift to higher values in the analytical model. We find that the analytical calculation systematically overestimates the RP when compared to our self-consistent numerical approach. This overestimation grows with increasing redshift.

(iii) The distribution of RP values experienced by satellite galaxies within $r_{\rm vir}$, estimated by both the gas-particles and the analytic methods, can be well fitted by Gaussian functions. The mean values of RP obtained from both methods are higher for the more massive clusters, a feature present for all redshifts. However, the difference between the two models becomes larger as one goes to higher redshifts, and with decreasing halo mass. This happens because the ICM density profiles in less massive clusters, and their progenitors at higher redshift, are galaxy-group sized systems of virial mass $\sim 10^{13}$–$10^{14}\,h^{-1}\,{\rm M}_{\odot}$, whose ICM distributions are not so well described by the analytical profile adopted. In the analytical model the evolution of the mean RP with redshift is milder, especially in the case of the G14 clusters.

(iv) For the gas-particles method, the RP values at $z = 0$ are weak ($4.68 \times 10^{-12}\,h^2\,{\rm dyn\,cm^{-2}}$) and medium ($3.09 \times 10^{-11}\,h^2\,{\rm dyn\,cm^{-2}}$) for G14 and G15 clusters, respectively. The majority of satellite galaxies in massive G15 clusters are already experiencing medium-level RP at $z \sim 2$, and at $z \lesssim 0.5$ about 20 per cent of satellites experience strong levels of RP (of order $10^{-10}\,{\rm dyn\,cm^{-2}}$). In the case of the G14 clusters, the mean RP is between medium and weak for $z \lesssim 1.5$, and few galaxies ever experience strong levels of RP; only at $z \sim 1$ does a significant fraction of satellites begin to experience medium levels of RP.

(v) Based on our self-consistent approach, we find that RPS has a strong effect on the cold gas content of galaxies in both sets of clusters. At $z = 0$ most galaxies ($\gtrsim$70 per cent) within $r_{\rm vir}$ are completely depleted of their cold star-forming gas. This is a strong difference with the model without RPS, where most galaxies manage to retain some cold gas: at the present epoch, only in the cluster cores ($r < 0.5r_{\rm vir}$) the fractions of gas-depleted galaxies reach ∼40 per cent. Observations of gas fractions as a function of clustercentric distance could provide strong constraints for the models.

(vi) The rate at which the cold gas is stripped from satellite galaxies depends on the virial mass of their host clusters. In our SAGRP model, the fractions of gas-depleted galaxies for G14 clusters increase appreciably between $z = 1$ and 0, whereas for G15 clusters the fractions at the present epoch are mostly established already at $z = 1$.

The general picture that emerges from the main results summarized above are that the RPS effect depends on halo virial mass and redshift, being more important in more massive haloes. Less massive galaxies within larger haloes are the most affected, so this could be the mechanism responsible for the transformation of dIrr galaxies into dSph in galaxy clusters (Boselli et al. 2008). In the more massive clusters the gas removal is extremely effective. RPS could contribute to the pre-processing of galaxies in smaller groups, before they fall into larger, cluster-sized systems.

ACKNOWLEDGMENTS

The authors thank Klaus Dolag for making the simulations available to them and for his help with this project, and the referee for useful suggestions and comments that improved this paper. TET wishes to thank Raúl Angulo, Carlton Baugh, Nelson Padilla and Leonardo Pellizza for their useful comments and discussions. SAC acknowledges Simon White for originally proposing the ideas that led to this project. This work was partially supported by PICT 245 Max Planck (2006) and PROALAR 2007.

REFERENCES

Abadi M. G., Moore B., Bower R. G., 1999, MNRAS, 308, 947
Abramson A., Kenney J. D. P., 2009, in Sheth K., Noriega-Crespo A., Ingalus J., Paladini R., eds, The Evolving ISM in the Milky Way and Nearby Galaxies, preprint, available online at http://ssc.spitzer.caltech.edu/mtgs/ismeuol
Agertz O. et al., 2007, MNRAS, 380, 963
Baldry I. K., Glazebrook K., Brinkmann J., Ivezić Ž., Lupton R. H., Nichol R. C., Szalay A. S., 2004, ApJ, 600, 681
Baldry I. K., Balogh M. L., Bower R. G., Glazebrook K., Nichol R. C., Bamford S. P., Budavari T., 2006, MNRAS, 373, 469
Balogh M. L., Navarro J. F., Morris S. L., 2000, ApJ, 540, 113
Balogh M. L., Baldry I. K., Nichol R., Miller C., Bower R., Glazebrook K., 2004, ApJ, 615, L101
Baugh C. M., Cole S., Frenk C. S., 1996, MNRAS, 283, 1361
Bekki K., Couch W. J., 2003, ApJ, 596, L13
Bett P., Eke V., Frenk C. S., Jenkins A., Helly J., Navarro J., 2007, MNRAS, 376, 215
Blumenthal G. R., Faber S. M., Flores R., Primack J. R., 1986, ApJ, 301, 27
Boselli A., Gavazzi G., 2006, PASP, 118, 517
Boselli A., Boissier S., Cortese L., Gil de Paz A., Seibert M., Madore B. F., Buat V., Martin D. C., 2006, ApJ, 651, 811
Boselli A., Boissier S., Cortese L., Gavazzi G., 2008, ApJ, 674, 742
Bower R. G., Benson A. J., Malbon R., Helly J. C., Frenk C. S., Baugh C. M., Cole S., Lacey C. G., 2006, MNRAS, 370, 645
Brüggen M., De Lucia G., 2008, MNRAS, 383, 1336 (BDL08)
Bruzual G., Charlot S., 2003, MNRAS, 344, 1000
Bullock J. S., Kolatt T. S., Sigad Y., Somerville R. S., Kravtsov A. V., Klypin A. A., Primack J. R., Dekel A., 2001, MNRAS, 321, 559
Ciardi B., Stoehr F., White S. D. M., 2003, MNRAS, 343, 1101
Cora S. A., 2006, MNRAS, 368, 1540
Cortese L., Gavazzi G., Boselli A., Franzetti P., Kennicutt R. C., O'Neil K., Sakai S., 2006, A&A, 453, 847

Cortese L. et al., 2007, MNRAS, 376, 157
Courteau S., Dutton A. A., van den Bosch F. C., MacArthur L. A., Dekel A., McIntosh D. H., Dale D. A., 2007, ApJ, 671, 203
Croton D. J. et al., 2006, MNRAS, 365, 11
Crowl H. H., Kenney J. D. P., van Gorkom J. H., Vollmer B., 2005, AJ, 130, 65
Davis M., Efstathiou G., Frenk C. S., White S. D. M., 1985, ApJ, 292, 371
De Lucia G., Blaizot J., 2007, MNRAS, 375, 2
Dolag K., Vazza F., Brunetti G., Tormen G., 2005, MNRAS, 364, 753
Dressler A., 1980, ApJ, 236, 351
Ellison S. L., Patton D. R., Simard L., McConnachie A. W., 2008, AJ, 135, 1877
Ellison S. L., Patton D. R., Simard L., McConnachie A. W., Baldry I. K., 2010, MNRAS, in press (arXiv:1002.4418)
Fall S. M., Efstathiou G., 1980, MNRAS, 193, 189
Faltenbacher A., Diemand J., 2006, MNRAS, 369, 1698
Flynn C., Holmberg J., Portinari L., Fuchs B., Jahreiß H., 2006, MNRAS, 372, 1149
Font A. S. et al., 2008, MNRAS, 389, 1619
Fujita Y., 2004, PASJ, 56, 29
Fujita Y., Nagashima M., 1999, ApJ, 516, 619
Gunn J. E., Gott J. R. I., 1972, ApJ, 176, 1 (GG72)
Haynes M. P., Giovanelli R., Chincarini G. L., 1984, ARA&A, 22, 445
Hopkins A. M., 2007, in Afonso J., Ferguson H. C., Mobasher B., Norris R., eds, ASP Conf. Ser. Vol. 380, Deepest Astronomical Surveys. Astron. Soc. Pac., San Francisco, p. 423
Hughes T. M., Cortese L., 2009, MNRAS, 396, L41
Impey C., Burkholder V., Sprayberry D., 2001, AJ, 122, 2341
Jáchym P., Palouš J., Köppen J., Combes F., 2007, A&A, 472, 5
Kapferer W., Sluka C., Schindler S., Ferrari C., Ziegler B., 2009, A&A, 499, 87
Kauffmann G., Colberg J. M., Diaferio A., White S. D. M., 1999, MNRAS, 303, 188
Kauffmann G., White S. D. M., Heckman T. M., Ménard B., Brinchmann J., Charlot S., Tremonti C., Brinkmann J., 2004, MNRAS, 353, 713
Kawata D., Mulchaey J. S., 2008, ApJ, 672, L103
Komatsu E., Seljak U., 2001, MNRAS, 327, 1353 (KS01)
Koopmann R. A., Kenney J. D. P., 2004, ApJ, 613, 866
Koopmann R. A., Kenney J. D. P., 2006, ApJS, 162, 97
Koopmann R. A., Haynes M. P., Catinella B., 2006, AJ, 131, 716
Kronberger T., Kapferer W., Ferrari C., Unterguggenberger S., Schindler S., 2008, A&A, 481, 337
Lagos C. D. P., Cora S. A., Padilla N. D., 2008, MNRAS, 388, 587 (LCP08)
Lanzoni B., Guiderdoni B., Mamon G. A., Devriendt J., Hatton S., 2005, MNRAS, 361, 369
Larson R. B., Tinsley B. M., Caldwell C. N., 1980, ApJ, 237, 692
McCarthy I. G., Frenk C. S., Font A. S., Lacey C. G., Bower R. G., Mitchell N. L., Balogh M. L., Theuns T., 2008, MNRAS, 383, 593
Macciò A. V., Dutton A. A., van den Bosch F. C., Moore B., Potter D., Stadel J., 2007, MNRAS, 378, 55
McConnachie A. W., Venn K. A., Irwin M. J., Young L. M., Geehan J. J., 2007, ApJ, 671, L33
Madau P., Ferguson H. C., Dickinson M. E., Giavalisco M., Steidel C. C., Fruchter A., 1996, MNRAS, 283, 1388
Marcolini A., Brighenti F., D'Ercole A., 2003, MNRAS, 345, 1329
Mastropietro C., Burkert A., Moore B., 2008, Publ. Astron. Soc. Australia, 25, 138
Mihos J. C., 2004, in Mulchaey J. S., Dressler A., Oemler A., eds, Clusters of Galaxies: Probes of Cosmological Structure and Galaxy Evolution. Cambridge Univ. Press, Cambridge, p. 277
Mo H. J., Mao S., White S. D. M., 1998, MNRAS, 295, 319 (MMW)
Moore B., Katz N., Lake G., Dressler A., Oemler A., 1996, Nat, 379, 613
Moore B., Lake G., Quinn T., Stadel J., 1999, MNRAS, 304, 465
Navarro J. F., Frenk C. S., White S. D. M., 1997, ApJ, 490, 493 (NFW)
Okamoto T., Nagashima M., 2003, ApJ, 587, 500
Perez M. J., Tissera P. B., Lambas D. G., Scannapieco C., 2006a, A&A, 449, 23
Perez M. J., Tissera P. B., Scannapieco C., Lambas D. G., de Rossi M. E., 2006b, A&A, 459, 361
Perez J., Tissera P., Padilla N., Alonso M. S., Lambas D. G., 2009, MNRAS, 399, 1157
Quilis V., Moore B., Bower R., 2000, Sci, 288, 1617
Roediger E., 2009, Astron. Nachrichten, 330, 888
Roediger E., Brüggen M., 2006, MNRAS, 369, 567
Roediger E., Brüggen M., 2007, MNRAS, 380, 1399
Roediger E., Hensler G., 2005, A&A, 433, 875
Schindler S., Binggeli B., Böhringer H., 1999, A&A, 343, 420
Schulz S., Struck C., 2001, MNRAS, 328, 185
Solanes J. M., Manrique A., García-Gómez C., González-Casado G., Giovanelli R., Haynes M. P., 2001, ApJ, 548, 97
Springel V., 2005, MNRAS, 364, 1105
Springel V., White S. D. M., Tormen G., Kauffmann G., 2001, MNRAS, 328, 726
Springel V. et al., 2005, Nat, 435, 629
Strateva I. et al., 2001, AJ, 122, 1861
Sun M., Donahue M., Voit G. M., 2007, ApJ, 671, 190
Sunyaev R. A., Norman M. L., Bryan G. L., 2003, Astron. Lett., 29, 783
Tormen G., Bouchet F. R., White S. D. M., 1997, MNRAS, 286, 865
Vikhlinin A., Kravtsov A., Forman W., Jones C., Markevitch M., Murray S. S., Van Speybroeck L., 2006, ApJ, 640, 691
Vollmer B., 2009, A&A, 502, 427
Vollmer B., Cayatte V., Balkowski C., Duschl W. J., 2001, ApJ, 561, 708
Warren M. S., Quinn P. J., Salmon J. K., Zurek W. H., 1992, ApJ, 399, 405
Wechsler R. H., Zentner A. R., Bullock J. S., Kravtsov A. V., Allgood B., 2006, ApJ, 652, 71
Whitmore B. C., Gilmore D. M., Jones C., 1993, ApJ, 407, 489
Yoshida N., Sheth R. K., Diaferio A., 2001, MNRAS, 328, 669

This paper has been typeset from a TEX/LATEX file prepared by the author.